CHAPTER 5

HYPERTENSION OF MIDDLE CEREBRAL ANEURYSM

Nadia Shaira Shafii[1,5], Muhammad Faiz Md Shakhih[1], Azah Muslim[2], Mohd Jamil bin Mohamed Mokhtarudin[1], Kahar Osman[2], Nofrizalidris Darlis[3]*

[1]Department of Biomedical Engineering and Health Sciences, Faculty of Electrical Engineering, Universiti Teknologi Malaysia, 81310 Johor, Malaysia

[2]Faculty of Mechanical Engineering, Universiti Teknologi Malaysia, 81310 Johor, Malaysia.

[3]Department of Mechanical Engineering Technology

Faculty of Engineering Technology, Universiti Tun Hussein Onn Malaysia, Pagoh Higher Education Hub, KM 1,

Jalan Panchor, 84600 Pagoh, Muar, Johor, Malaysia

[5]IJN-UTM Cardiovascular Engineering Center, Institute of Human Centered Engineering, Universiti Teknologi Malaysia, 81300 Skudai Johor

5.1 INTRODUCTION

Chalouhi et al. (2013) defined Cerebral aneurysms (CAs) are characterized by localized structural deterioration of the arterial wall, with loss of the internal elastic lamina and disruption of the media. While Meng et al. (2014) defined CAs or Intracranial Aneurysms (IAs) in simple way, they said intracranial aneurysm are pathologic outpunching of the arterial wall. Boussel et al. (2008) stated evolution of intracranial aneurysmal disease is known to be related to hemodynamic forces acting on the vessel wall. However, Taylor et al. (1995) stated that cerebral arterial aneurysms are common in the general population and their rupture is a catastrophic event. Chalouhi et al. (2013) studied that 3% to 5% of cerebral aneurysm occur in general population. In fact, the most dreaded complication of CAs is rupture, the likelihood of which is related to several modifiable and nonmodifiable risk factors (Chalouhi et al., 2013). Taylor et al. (1995) reported the role of systemic hypertension in aneurysm formation and rupture has been especially controversial. Patients' gender and race are not significant predictors of aneurysm rupture. Hypertension is an independent risk factor due to rupture of aneurysm in patient with unruptured cerebral aneurysm as their primary diagnosis.

With advances in computer technology, the behaviour of the rupture tendency in complex cerebral arterial models have been observed with aid of the computational fluid dynamics (CFD) technique. Thus, the aim of this study is to investigate the impact of various blood pressure condition to the flow behavior inside the aneurysm and the rupture risk.

5.2 METHODOLOGY

5.2.1 Image remodeling and meshing

In this study, a patient-specific model of middle cerebral artery (MCA) aneurysm is remodeled using computational aided design (CAD) software, SolidWork and used to ensure good accuracy of the results. Figure 5.1 shows the meshed geometry before boundary conditions are set to the model with about 600,000 nodes.

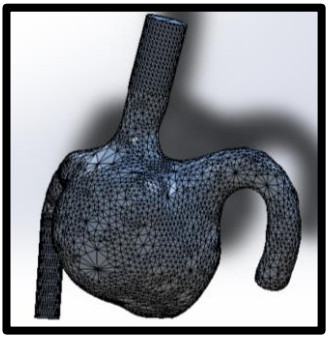

Figure 5.1: Meshed cerebral aneurysm geometry model

5.2.2 Numerical Modelling and Boundary Condition

The numerical simulation was carried out using ANSYS Fluent 19 software in steady state condition. In this study, blood properties were considered an incompressible Newtonian fluid with a density of 1056 kg/m^3 and a dynamic viscosity of 0.0035 kg/ms. To ensure the accuracy of the numerical results, a grid independence test was conducted,

and the optimal mesh count was selected for the final simulations. The turbulence model adopted for this study was the k-ω model. The MCA aneurysm model will be simulated with three different blood flow velocities as the inlet based on the findings of Azhim et al. (2011), while a free-flow condition was applied at the outlet. The specific blood pressure and flow velocity conditions are tabulated in Table 5.1.

Table 5.1: The blood pressure conditions and the blood flow velocity values.

Blood pressure condition	Normal	Pre-Hypertension	Hypertension
Blood flow velocity (m/s)	0.92	0.95	0.72

5.2.3 Analysis of Hemodynamic Parameters

There are three hemodynamic parameters analyzed in this study: velocity, wall shear stress, and pressure. These parameters are crucial in understanding the influence of blood flow dynamics on aneurysm stability under different physiological conditions, including normal (NML), pre-hypertension (PHP), and hypertension (HBP). Velocity distribution provides insight into flow patterns, vortex formation, and stagnation points within the aneurysm. Wall shear stress is essential for evaluating the forces exerted by blood flow on the arterial walls, which can affect endothelial function and aneurysm progression. Pressure distribution, particularly on the aneurysm wall, helps determine stress

accumulation, which may contribute to aneurysm growth and rupture risk.

$$v = \sqrt{v_x^2 + v_y^2 + v_z^2} \quad (1)$$

where v_x^2, v_y^2 and v_z^2 are the velocity components in the x, y and z directions, respectively. The flow structure was classified as complex, characterized by continuous recirculation at the bottom of the dome artery and flow separation toward multiple outlets. When observed from different angles, multiple vortices were evident around the aneurysm dome, further highlighting the intricate nature of the hemodynamic environment. WSS plays a crucial role in aneurysm progression, as low or oscillatory shear stress may contribute to endothelial dysfunction and wall weakening. The pressure acting on the aneurysm wall was analyzed using the pressure distribution computed directly in ANSYS Fluent post-processing. Regions of high-pressure concentration on the aneurysm wall indicate areas of increased mechanical stress, which may contribute to aneurysm expansion and rupture. By analyzing these hemodynamic factors, this study aims to provide a better understanding of the biomechanical factors influencing aneurysm stability and potential complication.

5.3 RESULTS AND DISCUSSION

This section presents the findings and analysis of the key hemodynamic parameters: velocity distribution, wall shear stress (WSS), and pressure variations within the aneurysm. These parameters were evaluated under three physiological conditions normal (NML), pre-hypertension (PHP), and hypertension (HBP) to investigate their impact on aneurysm stability and potential rupture risk.

5.3.1 Velocity Distribution

This section explains the velocity distribution under three conditions: normal, pre-hypertension, and hypertension. In the normal condition, blood flow remains stable with smooth velocity profiles and minimal turbulence. Under pre-hypertension, the flow velocity increases slightly, indicating elevated pressure effects on the vessel wall. In the hypertension condition, the velocity becomes significantly higher with stronger flow impact and disturbed patterns, suggesting increased hemodynamic stress within the aneurysm region. Figure 5.2 shows the velocity of blood flow in normal condition (0.92 m/s) in form of streamline. The red colour represent highest velocity, while dark blue colour represent lowest velocity. As shown in figure the blood flow velocity increasingly in inlet and in outlet instead of blood flow velocity decreasingly when in dome. In dome artery, blood flow keeps recirculating in low velocity before moving to outlet. Figure 5.3 and Figure 5.4 showed detailed streamline and contour of flow velocity at the middle cross plane.

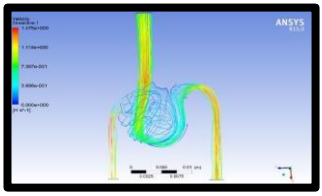

(a)

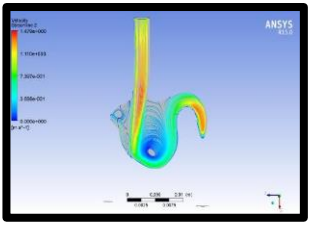

(b)

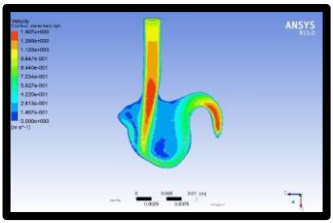

(c)

Figure 5.2: Blood flow velocity distribution at (a) Streamline in overall view; (b) Streamline on middle plane;(c) Velocity contour on middle plane during normal condition.

Figure 5.3 shows the velocity of blood flow in a pre-hypertension condition (0.95 m/s) in the form of streamlines. This pre-hypertension condition has the highest blood flow velocity compared to the other two conditions (normal and hypertension). As seen in the streamline figure, the highest velocity of blood flow is observed at the inlet and outlets. This is because blood flow increases as it enters the inlet and exits through the outlets. The streamline pattern of the highest velocity is more distinct compared to the high-velocity flow in normal and hypertension conditions. Meanwhile, the lowest blood flow velocity is mostly observed in the dome region, particularly at the bottom of the dome and in the artery between the dome and the parent artery. The blood continues to recirculate within the dome before moving into the outlets.

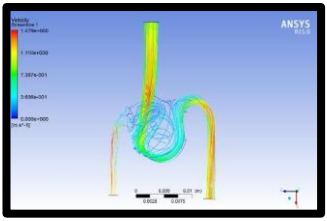

(a)

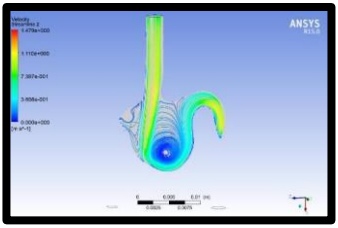

(b)

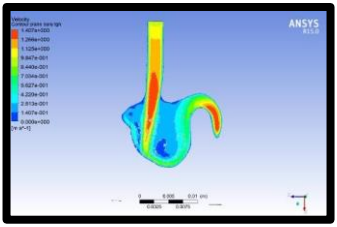

(c)

Figure 5.3: Blood flow velocity distribution at (a) Streamline in overall view; (b) Streamline on middle plane;(c) Velocity contour on middle plane during pre-hypertension condition.

Figure 5.4 shows the velocity of blood flow in a hypertension condition (0.72 m/s) in the form of streamlines. This hypertension condition has the lowest blood flow velocity compared to the normal and pre-hypertension conditions. As seen in the figure, only a few streamlines indicate high velocity values at the left outlet. The remaining streamlines appear green at the inlet and right outlet. Green-colored streamlines represent lower velocity values compared to yellow, orange, and red, which indicate progressively higher velocities. In the dome area, the velocity is at its lowest as the blood flow continues to recirculate before eventually moving out through the outlets.

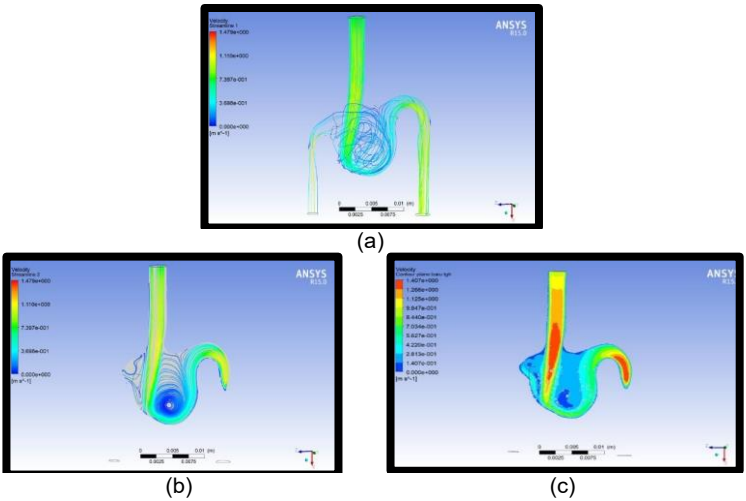

Figure 5.4: Blood flow velocity distribution at (a) Streamline in overall view; (b) Streamline on middle plane;(c) Velocity contour on middle plane during hypertension condition.

5.3.2 Wall Shear Stress

This section explains the wall shear stress (WSS) distribution under normal, pre-hypertension, and hypertension conditions. In the normal condition, WSS remains within a physiological range, indicating stable flow and minimal stress on the vessel wall. Under pre-hypertension, WSS increases moderately, reflecting higher flow velocity and pressure. In the hypertension condition, WSS rises sharply, especially near the aneurysm neck and dome, suggesting elevated hemodynamic stress that may contribute to vessel wall weakening and potential rupture risk. Next, Figure 5.5, shows wall shear stress at normal blood pressure condition in the form of a contour. Red colour indicates highest wall shear stress while dark blue colour indicates lowest wall shear stress. This figure shows the front

view of the geometry. By looking at the geometry, the inlet and the outlet are red, which means the inlet and the outlet are the highest wall shear stress region. While at the upper side of the dome shows a dark blue region, the lowest wall shear stress.

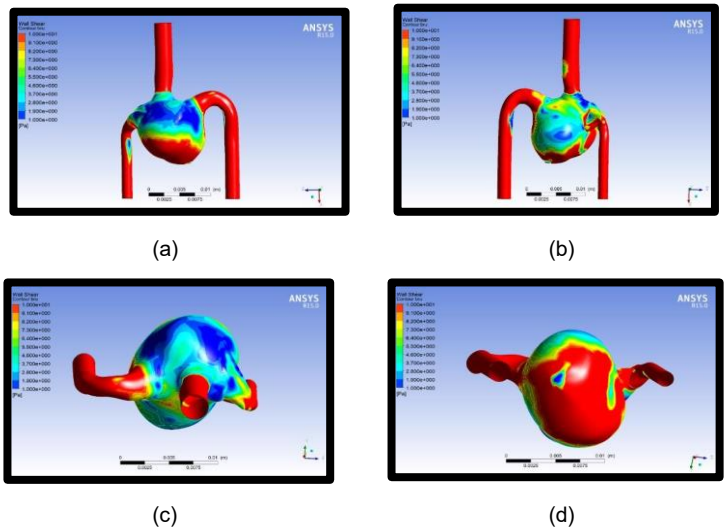

Figure 5.5: Wall shear stress distribution at (a) front view; (b) back view; (c) bottom view and (d) upper view for normal condition

For Figure 5.5 (b), it shows wall shear stress of geometry from the back view in the form of a contour. The inlet and outlet are red, which is at the highest wall shear stress region. While the lowest wall shear stress region is in the dome area, such as a small area at the right upper dome, a few spots at the left upper dome, and a slightly bigger region at the middle of the dome. Figure 5.5 (c) shows the wall shear stress of geometry in the form of a contour from the upper view. The upper part of the dome clearly shows the lowest wall shear stress regions. As shown in the figures, the lowest wall shear stress is found at

the upper dome, a slightly larger area at the right beside the inlet, and a few small spots left beside the inlet. The highest wall shear stress regions are still located at the inlet and both outlets. In Figure 5.5 (d), the geometry seen from bottom view in the wall shear stress measured, in the form of a contour. As seen in the figure, most of the bottom area, including outlets, is in the highest wall shear stress. However, the small spot area of lowest wall shear stress was generated and it is most noticeable because it was surrounded by high wall shear stress regions. The rupture tendency of aneurysms occurs in the lowest wall shear stress regions. Compared to the whole area in geometry, the dome area has a large area of low wall shear stress.

In Figure 5.6, the geometry illustrates the measurement of wall shear stress in the form of a contour from the front view. Compared to the normal condition, the area of lowest wall shear stress has slightly increased at the upper dome region. Additionally, a small spot at the left outlet has expanded, indicating a larger area of low wall shear stress. The inlet, most of the outlet region, and the bottom part of the dome remain areas of highest wall shear stress.

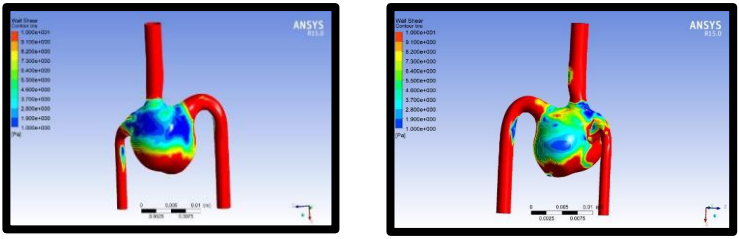

(a) (b)

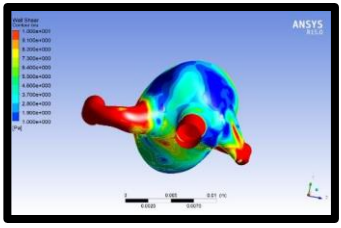

(c)

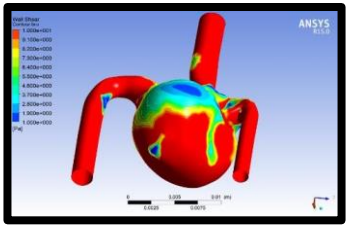

(d)

Figure 5.6: Wall shear stress distribution at (a) front view; (b) back view; (c) bottom view and (d) upper view for pre-hypertension condition

Figure 5.6 (b) presents the wall shear stress distribution from the back view. In the pre-hypertension condition, at the highest blood flow velocity, the lowest wall shear stress area in the dome region has slightly increased compared to the normal condition. The low wall shear stress area at the upper right of the dome has also expanded, with a few additional spots increasing in size. Blood flow velocity, influenced by blood pressure conditions, affects the wall shear stress in both the artery and the aneurysm regions. The areas in red remain indicative of the highest wall shear stress. Figure 5.6 (c) shows the wall shear stress distribution from the upper view. In the pre-hypertension condition, the regions with the lowest wall shear stress have increased in size. The dark blue spots, representing low shear stress areas, have also expanded. This occurs due to the increase in blood pressure from the normal to the pre-hypertension condition. Only the inlet and most of the outlet regions maintain high wall shear stress. Figure 5.6 (d) also displays the wall shear stress distribution from the upper view, reinforcing the findings from Figure 5.6(c). As in the pre-hypertension condition, the lowest wall shear stress regions have expanded, with dark blue spots increasing in size. This change is a result of rising blood pressure from the normal to

pre-hypertension condition. The inlet and most of the outlet regions continue to exhibit high wall shear stress.

Figure 5.7 shows the wall shear stress distribution in the form of a contour from the front view. As blood pressure increases, the area of lowest wall shear stress expands, spreading from the upper dome region to the upper area near the left outlet. Meanwhile, the inlet and the remaining outlet regions maintain the highest wall shear.

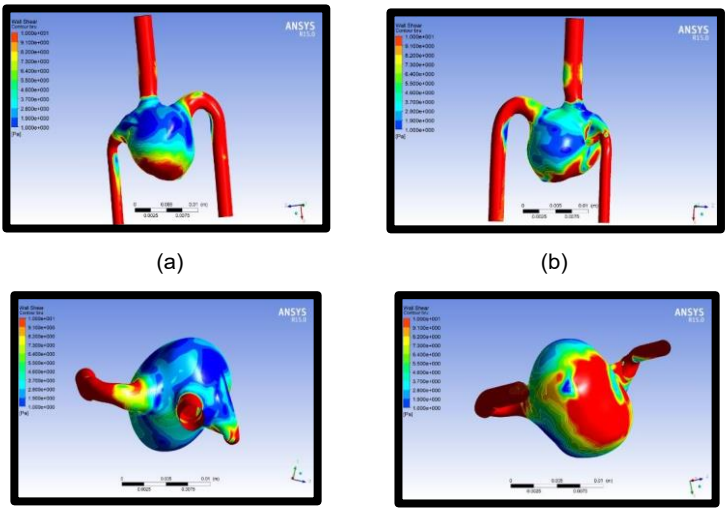

Figure 5.7: Wall shear stress distribution at (a) front view; (b) back view; (c) bottom view and (d) upper view for hypertension condition.

Figure 5.7 (b) shows the wall shear stress distribution in the form of a contour from the front view. As blood pressure

increases, the area of lowest wall shear stress expands, spreading from the upper dome region to the upper area near the left outlet. Meanwhile, the inlet and the remaining outlet regions maintain the highest wall shear stress. Figure 5.7 (c) illustrates the wall shear stress distribution from the upper view. It is clearly visible that the lowest wall shear stress region continues to expand, spreading widely around the upper dome area and extending to the neck between the lower part of the inlet and the upper part of the dome. This hypertension condition has a significant impact on the aneurysm. Figure 5.7 (d) presents the wall shear stress distribution from the bottom view. In both normal and pre-hypertension conditions, a small dark blue spot was already present. However, in the hypertension condition, this spot becomes noticeably larger compared to the previous conditions. This small spot forms due to the recirculation of blood flow within the dome and is referred to as the stagnation point. The stagnation point indicates a region with a higher tendency for rupture due to the presence of low wall shear stress. Low wall shear stress negatively affects endothelial cells and may contribute to local arterial wall remodeling. Meanwhile, high wall shear stress is represented by the red-colored regions.

5.3.3 Pressure During Normal, Pre-Hypertension and Hypertension Condition

Figure 5.8 (a) shows the pressure distribution in a cross-sectional plane of the geometry in the form of a contour for the normal condition. As clearly shown in the figure, the highest pressure occurs at the inlet entrance as blood begins to flow into the artery. Additionally, there is slightly higher pressure at the bottom of the dome area due to blood recirculating before moving into the outlets. As the blood passes through the outlets, the pressure gradually decreases as it exits the artery.

Figure 5.8(b) presents the pressure distribution in a cross-sectional plane for the pre-hypertension condition. Compared to the normal condition, the pre-hypertension condition exhibits higher pressure in the same areas, particularly at the inlet entrance and the bottom part of the dome. The red contour indicates a spike in pressure compared to the normal condition. This occurs because the blood flow velocity in pre-hypertension is higher than in the normal condition. Meanwhile, the pressure remains low at the outlets. Figure 5.8(c) shows the pressure distribution in a cross-sectional plane for the hypertension condition. As seen in the figure, there are no significantly high-pressure areas in this condition. Only bright green regions appear at the inlet entrance and the bottom of the dome, indicating slightly elevated pressure. In contrast, yellow, orange, and red colors, which represent higher pressure, are absent. In the hypertension condition, blood flow velocity is lower than in both the normal and pre-hypertension conditions. Meanwhile, the outlets remain at the lowest pressure as the blood flows outward.

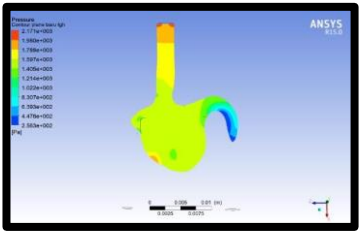

(a)

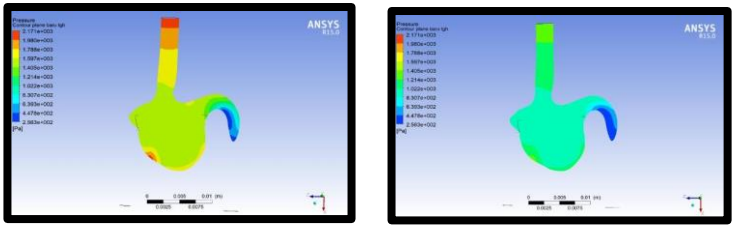

(b) (c)

Figure 5.8: Contour of pressure in a plane cross area during each timestep

5.4 CONCLUSION AND RECOMMENDATIONS

The distribution and magnitude of wall shear stress (WSS) play a critical role in the structural integrity of intracranial aneurysms, influencing their stability and potential for rupture. Higher WSS is typically associated with unruptured aneurysms, particularly in regions with high-velocity blood flow, whereas lower WSS is strongly correlated with rupture-prone areas, especially at the aneurysm dome. Computational fluid dynamics (CFD) analysis has demonstrated that a widespread low WSS region across the dome significantly increases the likelihood of aneurysm rupture. Studies have further emphasized that hemodynamic factors, particularly WSS, are as crucial as morphological features in assessing rupture risk. Notably, the WSS at the rupture point aligns with the minimum WSS observed at the dome, indicating that persistent low WSS contributes to the degenerative weakening of the aneurysmal wall. The rupture points are primarily located on the aneurysm dome, where WSS is at its lowest and blood flow velocity is significantly reduced. This localized decrease in blood flow velocity can result in flow stagnation, leading to endothelial cell apoptosis, inflammatory responses, and the release of biochemical mediators that contribute to aneurysm wall

degradation. Flow dynamics within the aneurysm exhibit complex patterns, characterized by multiple vortices and recirculation zones near rupture-prone regions, where vector velocity is lower than in other areas. These findings suggest that both low WSS and intricate flow structures play a crucial role in aneurysm rupture mechanisms. Understanding these hemodynamic behaviors provides valuable insight into aneurysm progression, emphasizing the need for WSS-based assessments in rupture risk evaluation.

This study suggests that blood pressure conditions play a significant role in aneurysm development and may influence the likelihood of rupture by altering key hemodynamic characteristics, such as complex flow patterns and markedly low wall shear stress (WSS). The findings demonstrate a clear correlation between regions of low WSS and aneurysm progression in intracranial aneurysms. These insights could be valuable in predicting the potential location and timing of aneurysm growth, aiding in therapeutic decision-making and surgical planning to improve patient outcomes.

5.5 ACKNOWLEDGEMENT

The authors thank to the Universiti Teknologi Malaysia (UTM) for practical sup

BIBLIOGRAPHY

[1] M. H. Babiker, B. Chong, L. F. Gonzalez, S. Cheema, and D. H. Frakes, “Finite element modeling of embolic coil deployment: Multifactor characterization of treatment effects on cerebral aneurysm hemodynamics,” J. Biomech., vol. 46, no. 16, pp. 2809–2816, 2013.

[2] J. L. Brisman, J. K. Song, and D. W. Newell, “Cerebral aneurysms,” N. Engl. J. Med., vol. 355, no. 9, pp. 928–939, 2006.

[3] A. Campi et al., “Retreatment of ruptured cerebral aneurysms in patients randomized by coiling or clipping in the International Subarachnoid Aneurysm Trial (ISAT),” Stroke, vol. 38, no. 5, pp. 1538–1544, 2007.

[4] N. Chalouhi, B. L. Hoh, and D. Hasan, “Review of cerebral aneurysm formation, growth, and rupture,” Stroke, vol. 44, no. 12, pp. 3613–3622, 2013.

5] V. K. Chivukula et al., “Lagrangian trajectory simulation of platelets and synchrotron microtomography augment hemodynamic analysis of intracranial aneurysms treated with embolic coils,” J. Biomech. Eng., vol. 143, no. 7, 2021.

[6] M. R. Levitt et al., “Computational fluid dynamics of cerebral aneurysm coiling using high-resolution and high-energy synchrotron X-ray microtomography: Comparison with the homogeneous porous medium approach,” J. Neurointerv. Surg., vol. 9, no. 8, 2017.

[7] N. Lin, K. S. Cahill, K. U. Frerichs, R. M. Friedlander, and E. B. Claus, “Treatment of ruptured and unruptured cerebral aneurysms in the USA: A paradigm shift,” J. Neurointerv. Surg., vol. 10, Suppl. 1, i69–i76, 2018.

[8] W. C. Merritt, H. F. Berns, A. F. Ducruet, and T. A. Becker, “Definitions of intracranial aneurysm size and morphology: A call for standardization,” Surg. Neurol. Int., vol. 12, 2021.

[9] P. D. Morris et al., “Computational fluid dynamics modelling in cardiovascular medicine,” Heart, vol. 102, no. 1, pp. 18–28, 2016.

[10] P. M. Munarriz, P. A. Gómez, I. Paredes, A. M. Castaño-Leon, S. Cepeda, and A. Lagares, “Basic principles of hemodynamics and cerebral aneurysms,” World Neurosurg., vol. 88, pp. 311–319, 2016.

[11] Y. Murayama et al., “Computational fluid dynamics as a risk assessment tool for aneurysm rupture,” Neurosurg. Focus, vol. 47, no. 1, Art. no. E12, 2019.

[12] T. Otani et al., “Computational study for the effects of coil configuration on blood flow characteristics in coil-embolized cerebral aneurysm,” Med. Biol. Eng. Comput., vol. 55, no. 5, pp. 697–710, 2017.

[13] M. S. A. Paisal, I. Taib, A. E. Ismail, and A. M. T. Arifin, “Numerical analysis on the effect of normotensive and hypertensive physiological conditions onto hemodynamic characteristics in stented carotid artery,” Int. J. Mech. Mechatron. Eng., vol. 19, no. 1, pp. 94–107, 2019.

[14] N. S. Shafii et al., “Hemodynamic and flow recirculation effect on rupture prediction of middle cerebral artery aneurysm,” J. Adv. Res. Fluid Mech. Therm. Sci., vol. 79, no. 1, pp. 1–16, 2020.

[15] Y. Umeda et al., “Computational fluid dynamics (CFD) using porous media modeling predicts recurrence after coiling of cerebral aneurysms,” PLoS One, vol. 12, no. 12, Art. no. e0190222, 2017.

[16] H. Yadollahi-Farsani, M. Herrmann, D. Frakes, and B. Chong, “A new method for simulating embolic coils as heterogeneous porous media,” Cardiovasc. Eng. Technol., vol. 10, no. 1, pp. 32–45, 2019.

[17] R. Yamaguchi et al., “Effects of elasticity on wall shear stress in patient-specific aneurysm of cerebral artery,” J. Flow Control Meas. Vis., vol. 7, no. 2, pp. 73–, 2019.